Journal of
Applied Remote Sensing

RemoteSensing.SPIEDigitalLibrary.org

Assessment of the CubeSat Infrared Atmospheric Sounder impact on global numerical weather prediction using observational system simulation experiments

Yan Zhou
Narges Shahroudi
Sid-Ahmed Boukabara
Kayo Ide
Tong Zhu
Ross Hoffman
Sean Casey
Flavio Iturbide-Sanchez

SPIE.

Yan Zhou, Narges Shahroudi, Sid-Ahmed Boukabara, Kayo Ide, Tong Zhu, Ross Hoffman, Sean Casey, Flavio Iturbide-Sanchez, "Assessment of the CubeSat Infrared Atmospheric Sounder impact on global numerical weather prediction using observational system simulation experiments," *J. Appl. Remote Sens.* **13**(3), 032508 (2019), doi: 10.1117/1.JRS.13.032508.

Assessment of the CubeSat Infrared Atmospheric Sounder impact on global numerical weather prediction using observational system simulation experiments

Yan Zhou,[a,b,*] Narges Shahroudi,[a,c] Sid-Ahmed Boukabara,[a] Kayo Ide,[d] Tong Zhu,[a,e] Ross Hoffman,[a,b] Sean Casey,[f,g] and Flavio Iturbide-Sanchez[a]

[a]NOAA/NESDIS/Center for Satellite Applications and Research (STAR), College Park, Maryland, United States

[b]University of Maryland, Earth System Science Interdisciplinary Center, College Park, Maryland, United States

[c]Riverside Technology Inc., Silver Spring, Maryland, United States

[d]University of Maryland, Department of Atmospheric and Oceanic Science, College Park, Maryland, United States

[e]Colorado State University, Cooperative Institute for Research in the Atmosphere, Fort Collins, Colorado, United States

[f]University of Miami, Cooperative Institute for Marine and Atmospheric Studies, Miami, Florida, United States

[g]NOAA/Atlantic Oceanographic and Meteorological Laboratory, Miami, Florida, United States

Abstract. The CubeSat Infrared Atmospheric Sounder (CIRAS) is a proposed small satellite IR sounder developed in response to the challenges of high cost and possible data gaps for currently operational hyperspectral IR sounders, such as Atmospheric Infrared Sounder, Infrared Atmospheric Sounding Interferometer, and Crosstrack Infrared Sounder. A key objective of CIRAS is to demonstrate the technologies required for a low cost-to-orbit, operational IR sounder. CIRAS was designed by National Aeronautics and Space Administration's Jet Propulsion Laboratory, with 625 channels measuring upwelling IR radiation of the Earth in the mid-wavelength IR spectrum region. Through observational system simulation experiments, the impact of assimilating CIRAS on global numerical weather prediction was assessed. CIRAS was simulated by applying the Community Radiative Transfer Model to profiles extracted from the Goddard Earth Observing System Model, Version 5 nature run for an afternoon polar orbiting sensor, and then assimilated by the National Centers for Environmental Prediction Global Data Assimilation System. Assimilating CIRAS improved global analysis and forecasts, when added to the currently operational observing configuration and to a data gap scenario. [DOI: 10.1117/1.JRS.13.032508]

Keywords: CubeSat; IR sounder; CubeSat Infrared Atmospheric Sounder; data assimilation; observational system simulation experiments; numerical weather prediction.

Paper 190163 received Mar. 19, 2019; accepted for publication Jun. 19, 2019; published online Jul. 23, 2019.

1 Introduction

Hyperspectral infrared (IR) sounders of the atmosphere, such as Atmospheric Infrared Sounder (AIRS), Infrared Atmospheric Sounding Interferometer (IASI), and Crosstrack Infrared Sounder (CrIS), have become a vital element in the observing systems for improving numerical weather prediction (NWP). For example, in the European Center for Medium-Range Weather Forecasts operational assimilation and forecast system, AIRS and IASI each accounted for 12% of the 24-h forecast error reduction during September to December 2008.[1] AIRS is expected to complete its mission by 2022. CrIS, IASI, and their nearly identical replacements are expected to operate into the late 2030s.[2] The cost of these legacy hyperspectral IR sounders is substantial, making it

*Address all correspondence to Yan Zhou, E-mail: yanzhou@umd.edu

1931-3195/2019/$28.00 © 2019 SPIE

difficult to justify launching them into multiple orbits to achieve higher spatial and temporal coverage. One approach to mitigate the challenges of high cost and possible data gaps for hyperspectral IR sounders in the future is to explore lower cost alternatives, such as the CubeSat Infrared Atmospheric Sounder (CIRAS). CIRAS is a mission that aims to demonstrate the technology enabling hyperspectral IR atmospheric sounding on a CubeSat. To do this, CIRAS relies on temperature and water vapor channels (listed in Sec. 6) in the spectral range 4.08 to 5.13 μm (or 2450 to 1950 cm^{-1}). There are multiple definitions of the mid-wavelength IR (MWIR) and short-wavelength IR (SWIR). We will refer to the CIRAS channels as MWIR, which is consistent with one common definition of the MWIR as the spectral region from 3 to 8 μm (or 3333 to 1250 cm^{-1}). The space industry traditionally produced sophisticated spacecraft within only a few large government-backed programs that employed large teams of scientists and engineers. However, there has been increasing interest in smaller missions over the last decade, inspired by advances in commercial-off-the-shelf miniaturization technologies.[3] CubeSats, as defined by National Aeronautics and Space Administration (NASA), "are a class of nanosatellites that use a standard size and form factor." They provide cost-effective platforms for science investigations, new technology demonstrations, and advanced mission concepts using constellations of satellites.[4]

This study aims to answer two questions. First, to what extent can CubeSat-based hyperspectral IR sounders mitigate the loss of afternoon polar orbit and all secondary satellites? Second, can CubeSat IR sounders contribute to improve global analysis and forecast performances compared with current satellite constellations? A set of global observing system (GOS) simulation experiments (OSSEs) was carried out to address these questions and assess the quantitative impact of observations from low-cost and small-size hyperspectral IR sensors. These experiments make consistent use of the Community Radiative Transfer Model (CRTM) for both simulating and assimilating IR brightness temperatures (BTs). No explicit random or bias errors are added to the simulated observations. For the MWIR, the solar source term is included, but NLTE effects are not. In an OSSE, observations are synthesized from one or more forecasts generated by a sophisticated NWP model, which statistically simulates the real atmosphere.[5] These independent forecasts, referred to as "nature runs" (NRs), are not identical to the real atmosphere but are statistically similar and are considered to be as the "truth," in the OSSE context. In the current study, the NR is the NASA 7-km resolution, nonhydrostatic Goddard Earth Observing System Model, Version 5 (GEOS-5) NR (G5NR).[6,7] The simulated observations are then used by an independent data assimilation (DA) system to quantitatively estimate NR states.

Section 2 describes the methodology, including a brief introduction of the Community Global OSSE Package (CGOP), experiment design, and assessment metrics. The simulated CIRAS dataset is discussed in Sec. 3, including CIRAS's specifications, description of the observation simulation process, and discussion about CIRAS channels selection for the OSSEs. The results of the OSSEs we performed, demonstrating the impact of CIRAS on global NWP, are presented in Sec. 4, followed by the discussion and conclusions given in Sec. 5.

2 Methodology

2.1 *CGOP for Hypothetical Observing Systems*

Boukabara et al.[8] developed the CGOP in response to the challenges of creating, maintaining, and validating a state-of-the-art OSSE system. Its key components include the NR (G5NR), the forward operators for data simulation, the National Centers for Environmental Prediction (NCEP) Global Forecast System (GFS), and the Global DA System (GDAS). The DA component employs the gridpoint statistical interpolation (GSI) analysis system.[9] The observation simulation process is an important component in CGOP, which has been validated by Boukabara et al.[10] The accuracy and reliability of the OSSE system conducted by CGOP have also been calibrated.[11]

The current study employed a research version of GDAS/GFS configuration with reduced resolution of T670 for the deterministic forecast, and T254 for the ensemble forecasts and DA.

The 64-layer sigma-pressure hybrid co-ordinate and 80-member ensembles are the same as the currently operational configuration. The 2015 operational DA scheme employed the same hybrid 3DEnVar version of the GSI.[12]

Although adding explicit errors to perfect simulation is important in matching the observing systems to reality,[13,14] real error characteristics of proposed observations are usually unknown. To treat the existing and the proposed observations consistently, no explicit errors were added to the perfect observations in this study. Using perfect observations means the instrument error is neglected, which will underestimate the error and uncertainty present in the real world.[5] Riishojgaard et al.[15] also recognized that one consequence of using perfect observations is the overestimation of forecast skill of the system. Despite all of the limitations, the relative impact of OSSEs assimilating perfect observation still shows equivalency to the relative impact observed in the real-data observing system experiments (OSEs).[11] This is sufficient when assessing the impact of satellite constellation changes.

The CIRAS observes MWIR spectral regions, where no hyperspectral radiances are used in current operational NCEP DA system. So, there is no direct way to assimilate CIRAS in GSI. A routine was added into the GSI source code for processing CIRAS observations in the same manner as processing CrIS. The estimated observation error standard deviation required by GSI for each selected CIRAS channel was taken from the corresponding CrIS or IASI channels.

2.2 *Experiment Design and Assessment Metrics*

A series of experiments were conducted to quantify the impact of CIRAS on global NWP under two baseline scenarios, Control and 2Polar. The Control run used all operational observations available to the GDAS/GFS in the January 2015 implementation. The 2Polar run was a data denial experiment with an observing system configuration in which the afternoon coverage provided by Suomi National Polar-orbiting Partnership (SNPP) and all secondary polar-orbiting platforms were removed, leaving only the observations from the operational early and midmorning platforms. Thus, 2Polar provides a benchmark for the assessment of mitigation strategies designed to reduce the negative impact associated with this data gap scenario. These two configurations (Control and 2Polar) were among the OSEs studies by Boukabara et al.[16] and the OSEs and OSSEs intercompared by Boukabara et al.[11] Table 1 summarizes the four OSSEs. All experiments in Table 1 were run from August 8 to August 14, 2006, as spin-up, and August 15 to September 15, 2006, as assessment period. The GDAS was cycled for four synoptic times at 0000, 0600, 1200, and 1800 UTC. The GFS 0 to 168 h forecasts were initialized by the 0000 UTC GDAS analysis every day during the assessment period. The assimilated observations included satellite radiances, Atmospheric Motion Vectors, Global Positioning System Radio Occultation, and conventional observations, such as radiosondes. The observations used in each experiment are presented in Fig. 1. Columns are for each OSSE experiment and rows for each type of observation. Green means that a given observation was used in the current experiment. All simulated observations are explicit-observation-error-free.

One of the main metrics that quantitatively estimates the impact of CIRAS on the global NWP analyses and forecasts is the overall score described in Boukabara et al.[16] (hereafter,

Table 1 List and description of the OSSE experiments.

Experiments	Observing system for each experiment
Control	Observing system in use in the 2015 operational implementation of GDAS/GFS
Control + CIRAS	Observing system of Control plus simulated CIRAS radiances on SNPP orbit
2Polar	Observing system of Control minus all secondary and afternoon polar-orbiting platforms, leaving only two remaining polar platforms, F18 (early morning) and MetOp-B (mid-morning)
2Polar + CIRAS	Observing system of 2Polar plus simulated CIRAS radiances on SNPP orbit

PLATFORM (SENSOR)	Control	Control+ CIRAS	2Polar	2Polar+ CIRAS
DMSP-F16 (SSMI/S)				
DMSP-F17 (SSMI/S)				
DMSP-F18 (SSMI/S)				
N15, N18, N19 (AMSU)				
AQUA (AIRS,AMSUA)				
MetOp-A (AMSU,MHS,IASI,HIRS)				
MetOp-B (AMSU,MHS,IASI)				
SNPP(ATMS)				
SNPP(CrIS)				
GOES 15(SNDRS)				
M10 (SEVIRI)				
COSMIC, MetOp-A, MetOp-B, TSX, GRACE				
Satellite Wind				
Conventional Wind				
Moisture				
Surface Pressure				
Temperature				
SNPP(CIRAS)				

Fig. 1 Observations usage in OSSE experiments. Columns are for each OSSE experiment, and rows for each type of observations. Green (red) refers that one observation was used in current experiment.

BGK). BGK estimated the impact of plausible degradation in the GOS on global NWP forecast skill, as current satellite missions transition to the next generation of sensors. BGK introduced the overall forecast scores (OFS), which was computed by combining the primary forecast verification metrics, namely the anomaly correlation (AC) and root mean square error (RMSE), for all parameters, atmospheric levels, and forecast lead times. With the same idea of OFS, the global analysis quality of each OSSE in the current research can be represented by the overall analysis score (OAS). Other assessment methods include bias, RMSE, and scorecards created by National Oceanic and Atmospheric Administration/NCEP/Environmental Modeling Center standard operational verification statistics database (VSDB) system.

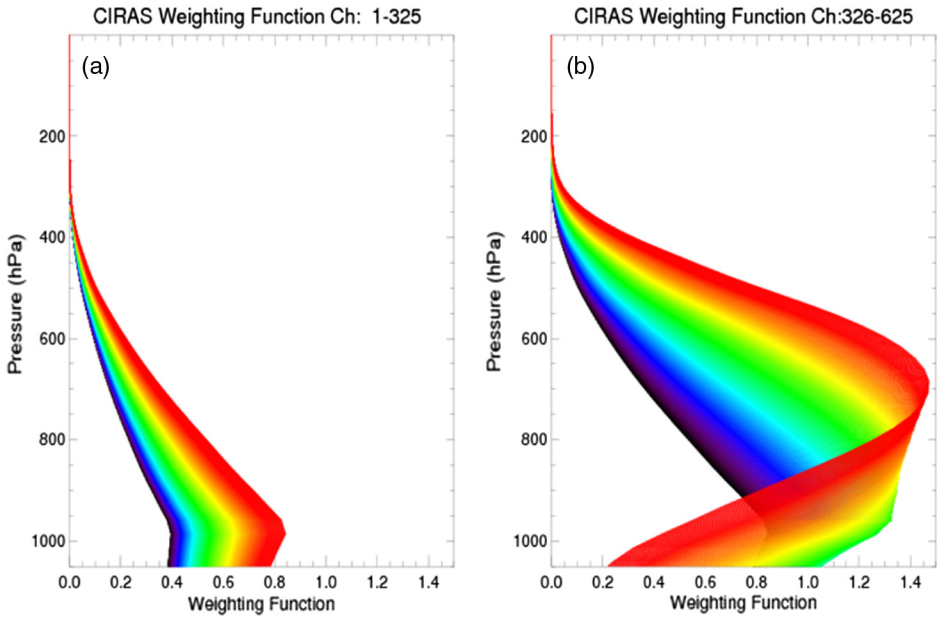

Fig. 2 Weighting function of CIRAS for (a) channels 1 to 325, 2449.91 to 2162.07 cm^{-1} and (b) channels 326 to 625, 2161.29 to 1949.95 cm^{-1}. Cooler colors indicate shorter wavelengths.

3 Data

3.1 *CIRAS Instrument Design*

CIRAS is a hyperspectral IR sounder designed by NASA's Jet Propulsion Laboratory, managed by the California Institute of Technology. It has 625 channels and measures upwelling IR radiation of the Earth in the mid-wavelength IR (MWIR) spectrum region (1950 to 2450 cm^{-1} or 4.08 to 5.13 μm, with spectral resolution of 1.2 to 2.0 cm^{-1}). A key objective of CIRAS is to demonstrate the technologies required for a low cost-to-orbit, operational IR sounder, the Earth Observing Nanosatellite-IR. The key in-space technologies required for hyperspectral IR measurements include the high operating temperature barrier IR detector, the coaxial micro pulse tube cryocooler, MWIR grating spectrometer, and black silicon IR blackbody.[17] The weighting functions of CIRAS are given in Fig. 2(a) (channels 1 to 325, 2449.91 to 2162.07 cm^{-1}) and Fig. 2(b) (channels 326 to 625, 2161.29 to 1949.95 cm^{-1}), with cooler colors indicating shorter wavelengths. The observed radiances can be used to retrieve temperature and water vapor information in the troposphere and thus to support weather and climate science investigations.

3.2 *CIRAS Data Simulation and Validation*

The processes of simulating observations were described in Sec. 4 of Boukabara et al.[8] The main steps include (1) interpolation of the NR to the observing locations, (2) invocation of forward operators, (3) creation of "perfect" observations (error-free except for systematic errors coming from the interpolation from the NR and the conversions by the forward operators), (4) addition of explicit errors, and (5) creation of simulated observations in Binary Universal Form for Representation of Meteorological Data (BUFR) format. For a hypothetical sensor, additional processes are required, such as defining the orbital configuration (observation time, geolocations, geometry, etc.); generating CRTM[18,19] optical depth coefficient files for radiance simulation; developing BUFR files; and specifying the observation errors. In this study, the CIRAS orbital configuration and data locations are taken to be that of real SNPP/CrIS data during the 8 August to 15 September, 2014 period. However, G5NR is not available for 2014. G5NR consists of 2-year global simulations covering the period from May 2005 to May 2007. We changed the year in the real SNPP/CrIS files from 2014 to 2006, but keep the same geolocations and observing geometry, such as satellite zenith angle and field-of-view. The CIRAS data were simulated on SNPP orbit in clear sky conditions from August 8 to September 15, 2006. These datasets represent the so-called "perfect observations" since no explicit errors have been added. Figure 3 shows the simulated CIRAS BT observations for August 8, 2008 00 UTC, for channel 39 (2412.25 cm^{-1}), a lower tropospheric temperature sounding channel.

The CIRAS proxy data were validated by comparing with AIRS simulations (Fig. 4) and real AIRS observations for the initial day of G5NR, May 16, 2005 (Fig. 5). The initial day of the

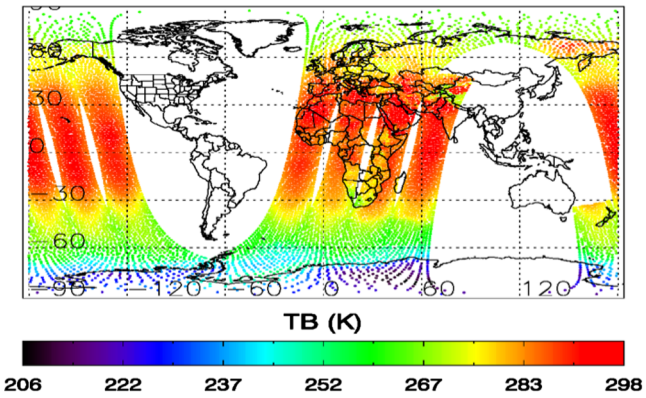

Fig. 3 Brightness temperature (K) of CIRAS channel 39 simulation on SNPP orbit (2412.25 cm^{-1}) for August 8, 2006, 00UTC.

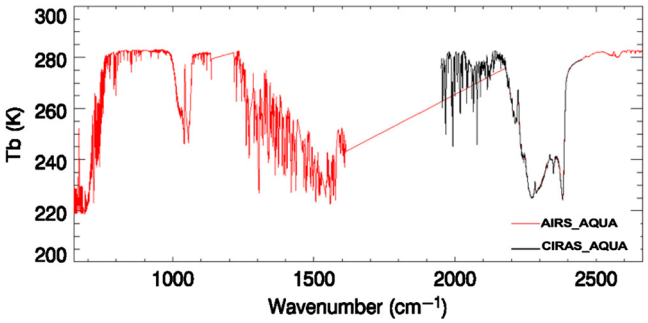

Fig. 4 The simulated brightness temperatures, T_b (K), with CRTM standard testing profiles for AQUA/AIRS (red) and CIRAS (black).

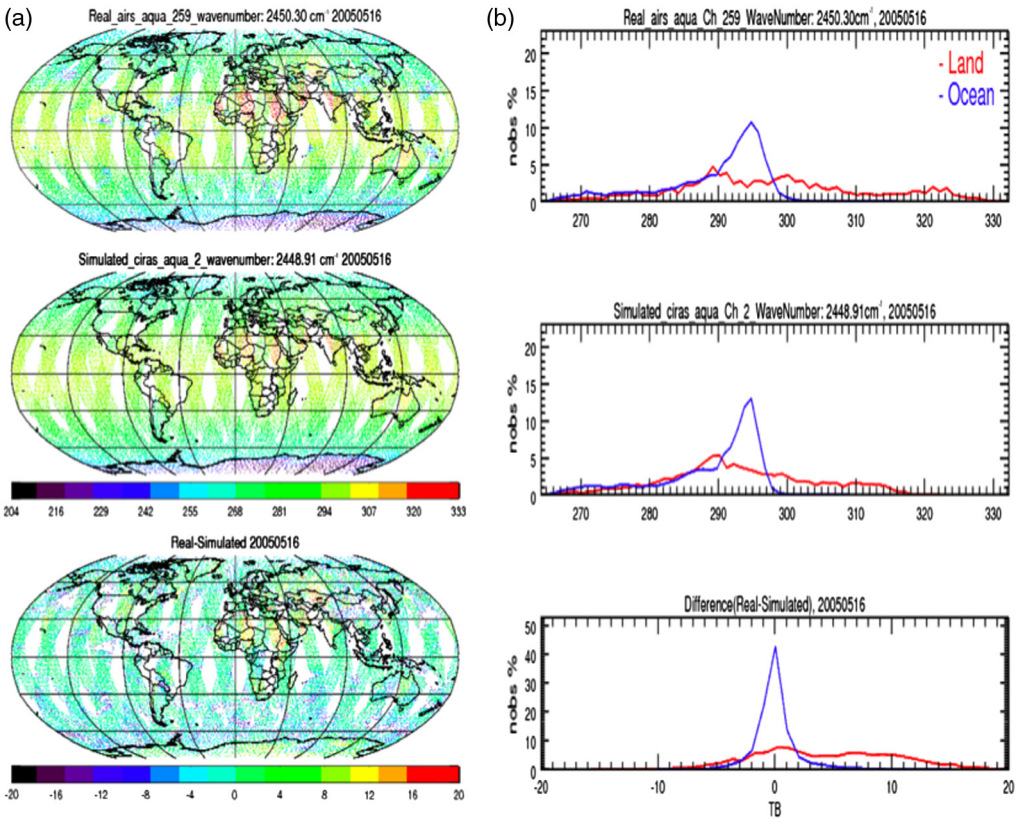

Fig. 5 (a) Maps and (b) histograms of CIRAS on Aqua orbit (2448.91 cm^{-1}) with real AQUA/AIRS (2450.30 cm^{-1}) for the G5NR initial day, 20050516. Maps are all sky globally, and histograms are for clear sky conditions and separated by land (red) and ocean (blue). For both (a) and (b), top panels are real AIRS, the middle panels are CIRAS perfect simulated observations, and the bottom panels are their difference (real AIRS minus simulated CIRAS).

G5NR is close enough to the real atmosphere state to make a direct comparison useful.[10] The AIRS was chosen for the validation because no other real IR hyperspectral observations were available at this time. Figure 4 shows the simulated nighttime (i.e., no solar source term) IR spectra for AIRS (red) and CIRAS (black), using the standard CRTM test profiles. There is good agreement in the spectral range, where AIRS and CIRAS overlap, which is sensitive to trace gases like carbon monoxide, carbon dioxide, and nitrous oxide (CO, CO_2, and N_2O). Figure 5 displays (a) maps and (b) histograms for two matching channels on Aqua orbit—simulated CIRAS channel 259 at 2448.91 cm^{-1} and observed AIRS channel 2 at 2450.30 cm^{-1}—for

the G5NR initial day. Maps are for all-sky conditions. Histograms are for clear sky conditions for land (red) and ocean (blue). For both panels (a) and (b), the top panels correspond to real AIRS, the middle panels are CIRAS perfect simulated observations, and the bottom panels are the real AIRS minus simulated CIRAS difference. The most notable difference between CIRAS and AIRS occurs over land and is mainly due to large uncertainties in land surface emissivity specified by CRTM.[20] However, and for this reason, IR BTs affected by the surface are assimilated only over the ocean in most operational DA and in our experiments.

3.3 *CIRAS Data Channel Selection*

The large volume of high spectral resolution IR radiance observations presents several challenges, including data transmission, storage, and assimilation. Using the full spectrum of hyperspectral IR data is not operationally feasible, and a simple approach is to identify a subset of channels that capture most of the information for the target parameters, such as temperature and water vapor. Rabier et al.,[21] Collard,[22] Ventress and Dudhia,[23] and Gambacorta and Barnet[24] discussed the methodologies of IASI and CrIS channel selection for use in NWP. For CIRAS, a subset of 101 channels was chosen from its full 625 channels to be assimilated. Table 3 lists the selected CIRAS channels with their corresponding CrIS or IASI channels of similar wavenumbers as well as the atmospheric sensitivity of each channel. The selected CIRAS channels matched with 78 CrIS channels sensitive to temperature and trace gases like CO, CO_2, and N_2O, and with 23 IASI channels sensitive to water vapor. Here, it is important to highlight that the current practice is to ignore SWIR radiances and, thus, none of the matching CrIS and IASI channels are currently operationally assimilated by NCEP. One purpose of the present study is to explore the potential benefits of using these channels. These channels are ignored primarily due to the computational expense and difficulties in characterizing the interaction of solar radiation with clouds and land surfaces. These data might be used during nighttime and/or for cloud detection and clearing.

4 Results

One advantage of OSSEs is that the "true" state of the atmosphere, or the NR, from which the observations are simulated is perfectly known. The global analyses and forecasts from OSSE experiments in this study are verified with respect to the NR.

The difference of the absolute values of the 250-hPa temperature analysis bias with respect to the NR is presented in Fig. 6 for (a) Control minus Control + CIRAS and (b) 2Polar minus 2Polar +CIRAS, where the biases are averaged for all four synoptic times between August 15 and September 15, 2006. Positive changes indicate improvement, i.e., a smaller bias after including CIRAS in addition to either Control [Fig. 6(a)] or 2Polar [Fig. 6(b)]. In general, improvements are seen, especially over the Tropics, although there are some areas showing negative impacts in

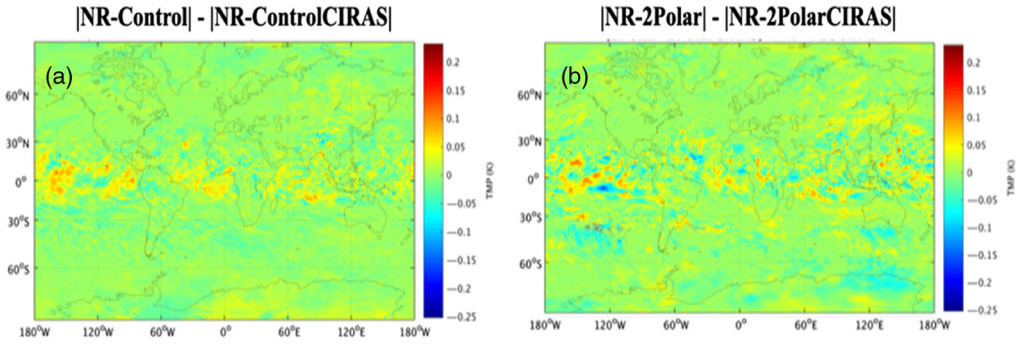

Fig. 6 The absolute values of the 250 hPa temperature analysis bias with respect to the NR for the difference of bias (a) between Control and Control + CIRAS, and (b) between 2Polar and 2Polar + CIRAS. Averaged for all four synoptic times between August 15 and September 15, 2006.

Fig. 6(b), for the 2Polar case. The improvements are small in magnitude but are widespread and based on an entire month of DA cycles.

The general positive impact of CIRAS on global NWP forecasts is seen in the scorecards presented in Figs. 7 and 8. Each of the scorecards compares two experiments (e.g., Control and Control + CIRAS in Fig. 7) using GFS forecasts for days 1, 3, 5, and 6 (or forecast hours 24, 72, 120, and 144), respectively, initialized each day at 0000 UTC from August 15 to September 15, 2006. The metrics include AC and RMSE for different variables—geopotential height (height), vector wind, and temperature (temp)—at different vertical levels, over different regions—North America, Northern Hemisphere, Southern Hemisphere, and the Tropics. Colors and shapes reflect the improvement or degradation. For example, in Fig. 7, large green (red) triangles denote that Control + CIRAS is better (worse) than Control at the 99.9% significance level; small green (red) triangles that Control + CIRAS is better (worse) than Control at the 99% significance level; light green (red) blocks that Control + CIRAS is better (worse)

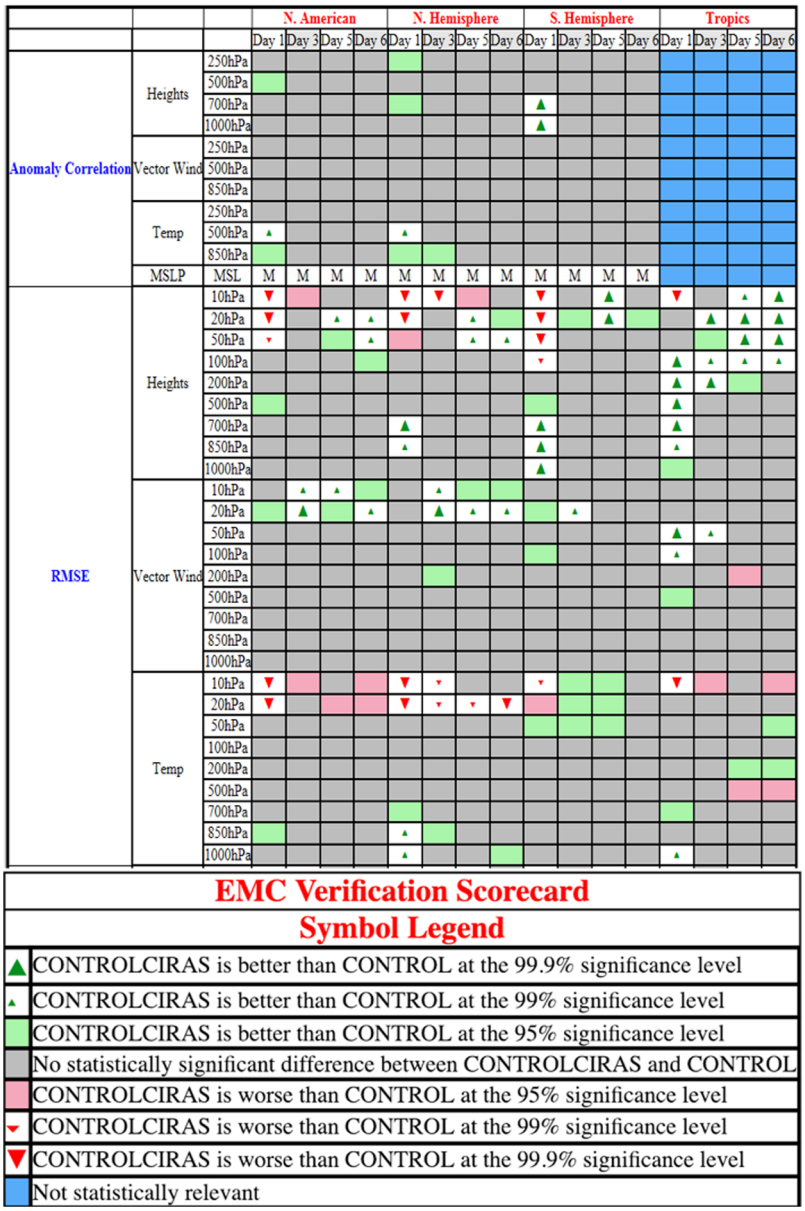

Fig. 7 VSDB Scorecards. Control versus Control + CIRAS for every 0000 UTC verified against NR, August 15 to September 15, 2006.

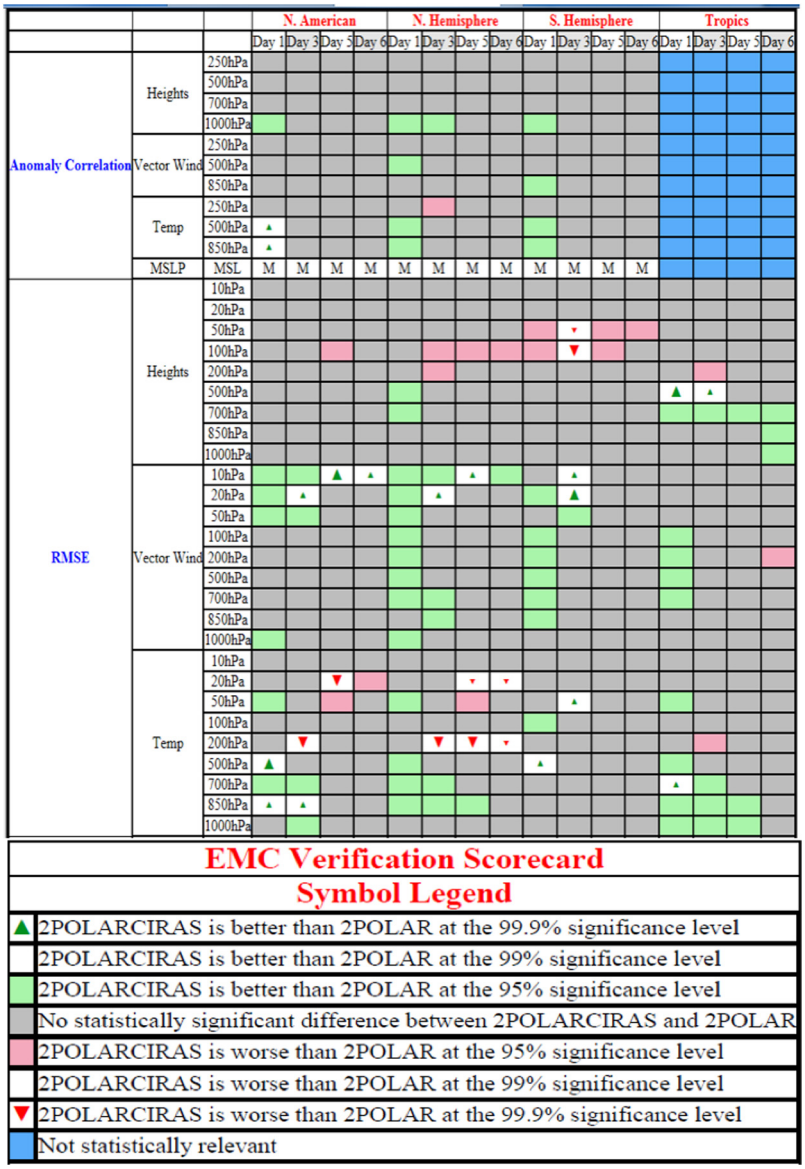

Fig. 8 VSDB scorecards. 2Polar versus 2Polar + CIRAS for every 0000 UTC verified against NR, August 15 to September 15, 2006.

than Control at the 95% significance level; gray blocks that there is no statistically significant difference between Control and Control + CIRAS; blue blocks that the value is not statistically relevant; and *M* that no MSLP data are available.

Only some of the impacts are significant, including the following: Control + CIRAS shows positive impact on AC for all variables for day 1 forecasts, and on RMSE for vector wind over all regions, mainly at mid-upper levels. The RMSE for geopotential height from Control + CIRAS shows general positive impact. However, note the negative impacts in Fig. 7 for geopotential height and temperature RMSE at levels above the peaks of the weighting functions (seen in Fig. 2). 2Polar + CIRAS shows positive impact on AC for all variables for day 1 and again, some negative impact on geopotential height in stratosphere is seen. There are improvements in vector wind and temperature RMSE, especially for days 1 and 3 (Fig. 8).

The global mean RMSE values of Control and Control + CIRAS analyses for HGT, Temp, vector wind, and relative humidity (RH) are shown in Table 2, at 250 and 500 hPa levels, over North and South Hemisphere, verified against NR every 6 h and averaged over August 15 to September 15, 2006. A green change signifies that assimilation of CIRAS improves the analysis, whereas a red change signifies that the assimilation of CIRAS degrades the analysis. The

Table 2 The extratropical mean RMSE values of Control and Control + CIRAS analyses for geopotential height (HGT), temperature (Temp), vector wind, and RH, at 250and 500 hPa levels, over North and South Hemisphere, verified against NR for every 6 h and averaged over August 15 to September 15, 2006. In the table, an italicized entry signifies CIRAS assimilation brings the analysis closer to the NR than the Control, and a bold entry signifies that the CIRAS assimilation pulls the analysis further away from the NR than the Control.

		North hemisphere		South hemisphere	
		Control	Control + CIRAS	Control	Control + CIRAS
HGT (m)	250 hPa	4.919	**4.925 (+0.1%)**	4.454	*4.442 (−0.3%)*
	500 hPa	3.545	*3.484 (−1.7%)*	4.018	**4.027 (+0.2%)**
Temp (K)	250 hPa	0.344	0.344 (0.0%)	0.411	**0.414 (+0.7%)**
	500 hPa	0.511	*0.502 (−1.8%)*	0.667	*0.657 (−1.5%)*
Vector Wind (m/s)	250 hPa	1.915	*1.913 (−0.1%)*	2.037	**2.044 (+0.3%)**
	500 hPa	1.826	*1.820 (−0.3%)*	2.344	*2.343 (−0.04%)*
RH (%)	250 hPa	11.606	*11.504 (−0.9%)*	9.836	*9.799 (−0.4%)*
	500 hPa	10.101	*9.998 (−1.0%)*	11.374	*11.355 (−0.2%)*

percentage in parentheses are the changes in RMSE due to including CIRAS. Most of the metrics in Table 2 show a positive impact of adding CIRAS to the Control configuration (i.e., a smaller analysis RMSE). The biggest positive impacts are for the 500 hPa HGT in NH, and the 500 hPa temperature in both NH and SH. While none of the changes in Table 2 are statistically significant at a 95% significance level, they are mostly positive especially for the Control versus Control + CIRAS comparisons.

Figure 9 shows the (a) OAS and (b) OFS for Control (green), Control + CIRAS (red), 2Polar (orange), and 2Polar + CIRAS (blue). The OAS and OFS were calculated using the metrics calculated by VSDB, including global AC for geopotential height, temperature, and vector wind at 250 and 500 hPa, and global RMSE for geopotential height, temperature, vector wind, and relative humidity at 250 and 500 hPa. The forecast scores were computed by combining forecast hours 0, 24, 48, 72, 96, 120, 144, and 168. The lower tropospheric metrics were excluded. At locations reporting below surface pressure (usually under 700 hPa), the differences in how

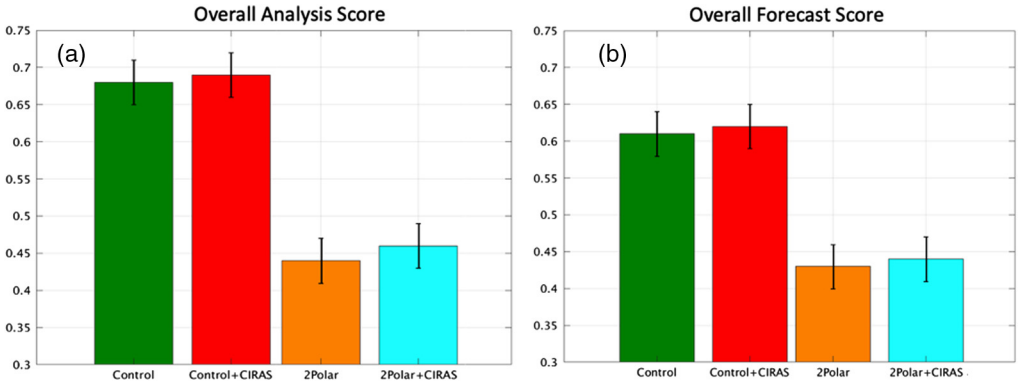

Fig. 9 The OAS (a) and OFS (b) for Control (green), Control + CIRAS (red), 2Polar (orange), and 2Polar + CIRAS (blue). Overall scores were computed for the period August 15 to September 15, 2006 using global AC for geopotential height, temperature, and vector wind at 250 and 500 hPa; global RMSE for geopotential height, temperature, vector wind, and relative humidity at 200 and 500 hPa. The forecast scores were computed by combining forecast hours 0, 24, 48, 72, 96, 120, 144, and 168.

analysis and forecasts are extrapolated for G5NR and GFS influence the calculated lower tropospheric AC and RMSE. In Fig. 9, the black error bars represent 95% confidence interval. The OAS and OFS of 2Polar are significantly smaller than those of Control, indicating that the removal of all secondary and afternoon polar orbits results in a significant degradation of global analysis and forecasts. The OAS and OFS of 2Polar + CIRAS are slightly larger than those of 2Polar but still significantly smaller than Control. This result clearly indicates that the loss of secondary and afternoon polar orbiting satellites was only partially compensated by CIRAS. The OAS and OFS of Control + CIRAS are slightly larger than those of Control, showing that including CIRAS has positive impacts on global analysis and forecast performances compared with current satellite constellations. The positive impacts are coming mainly from improvements over the Tropics and day-1 forecasts (Figs. 6 and 7). However, the positive changes in OAS and OFS are not significant.

5 Discussion and Conclusions

In this study, we have assessed the impact of a proposed small satellite hyperspectral IR Sounder, CIRAS, on global analyses and forecasts using OSSEs. CIRAS's impacts on two scenarios were investigated. First, experiment Control uses the complete currently operational satellite constellations implemented in the GDAS/GFS. Second, experiment 2Polar removes all secondary and afternoon polar orbits from satellite constellations of Control, retaining just two polar orbiting satellites (F18 and MetOp-B). Experiments Control + CIRAS and 2Polar + CIRAS are two OSSEs with CIRAS (simulated on the SNPP afternoon orbit) added to the Control and 2Polar satellite constellations, respectively. The global analyses and forecasts (out to 168 h) from each of these OSSEs were verified with respect to G5NR. The 2Polar configuration, as expected, showed the largest degradation for both analysis and forecasts comparing with Control (statistically significant at 95% level). With the addition of CIRAS to the 2Polar satellite configuration, global analysis and forecast performances were improved, but these improvements were not statistically significant. This suggested that CIRAS only partially mitigated the loss of secondary and afternoon polar orbiting satellites. CIRAS showed positive impact on global analysis and forecasts when added to the Control satellite configuration as well. The positive impacts of CIRAS on global forecast mainly come from the improvement over Tropics and day 1 forecasts. However, this improvement was not significant at the 95% level.

It should be noted that OSSE systems have limitations to assess the actual impact of real observations. Characteristics of the OSSE system used in this work need to be considered since they limit to some extent our ability to fully explore the capabilities of CIRAS, including: (1) the G5NR is cloudier than reality and the vertical distribution of cloud is not sufficiently realistic;[8] (2) our experiments considered only a single, as opposed to several CIRAS sensor(s); and (3) the current version of CRTM does not include nonlocal thermodynamic equilibrium (NLTE) effects, which impact IR sensor simulation primarily in the CO_2 spectral region at 4.3 μm.[25] In this study, cloud effects were not taken into account because radiances were simulated, both in the NR and in the GDAS, in noncloudy conditions. The actual impact of NLTE effects is not assessed due to limitations of CRTM. In reality, improved all-sky and NLTE radiance calculations will be needed to optimize the impact of CIRAS. Considering their relatively low expected costs with respect to conventional instruments, the full impact of CIRAS should be examined in experiments with a constellation of multiple CIRAS instruments. For example, the present study did not explore other possible CIRAS constellations, including perhaps 4 and 11 AM/PM orbits, which would certainly be helpful in nowcasting applications and very likely be useful in short-range high-resolution NWP. In addition, the present study did not consider other possible CubeSat solutions that would use alternative or additional spectral bands.

6 Appendix A

CIRAS selected channels, wavenumbers, and atmosphere sensitivity, with their corresponding CrIS or IASI channels of similar wavenumbers, are provided in Table 3. The selected CIRAS channels matched with 78 CrIS channels and 23 IASI channels.

Table 3 CIRAS selected channels, wavenumbers, and atmosphere sensitivity, with their corresponding CrIS or IASI channels of similar wavenumbers.

	CIRAS channel	CIRAS wavenumber	CrIS channel	CrIS wavenumber	Channel sensitivity
1	39	2412.25	1250	2412.50	T
2	46	2405.44	1247	2405.00	T
3	52	2399.63	1245	2400.00	CO_2
4	54	2397.70	1244	2397.50	T
5	57	2394.81	1243	2395.00	T
6	59	2392.89	1242	2392.50	T, CO_2
7	62	2390.01	1241	2390.00	T
8	67	2385.23	1239	2385.00	T, CO_2
9	70	2382.37	1238	2382.50	T
10	72	2380.47	1237	2380.00	T
11	75	2377.62	1236	2377.50	T, CO_2
12	78	2374.78	1235	2375.00	T
13	80	2372.89	1234	2372.50	T
14	86	2367.24	1232	2367.50	T
15	88	2365.36	1231	2365.00	T
16	94	2359.74	1229	2360.00	T
17	96	2357.88	1228	2357.50	T
18	102	2352.30	1226	2352.50	CO_2
19	107	2347.67	1224	2347.50	T
20	113	2342.13	1222	2342.50	T
21	118	2337.54	1220	2337.50	T
22	124	2332.05	1218	2332.50	T, CO_2
23	126	2330.23	1217	2330.00	T
24	132	2324.78	1215	2325.00	T
25	134	2322.97	1214	2322.50	T
26	140	2317.55	1212	2317.50	T
27	146	2312.16	1210	2312.50	T
28	151	2307.68	1208	2307.50	T
29	154	2305.01	1207	2305.00	T
30	157	2302.34	1206	2302.50	T
31	162	2297.90	1204	2297.50	T
32	165	2295.25	1203	2295.00	T
33	168	2292.60	1202	2292.50	T
34	174	2287.32	1200	2287.50	T

Table 3 (*Continued*).

	CIRAS channel	CIRAS wavenumber	CrIS channel	CrIS wavenumber	Channel sensitivity
35	177	2284.69	1199	2285.00	T
36	180	2282.07	1198	2282.50	T
37	182	2280.32	1197	2280.00	T
38	185	2277.71	1196	2277.50	T
39	191	2272.50	1194	2272.50	T
40	194	2269.91	1193	2270.00	T
41	197	2267.32	1192	2267.50	T
42	203	2262.16	1190	2262.50	T
43	206	2259.58	1189	2260.00	T
44	211	2255.31	1187	2255.00	T
45	229	2240.06	1181	2240.00	N_2O
46	232	2237.54	1180	2237.50	N_2O
47	235	2235.02	1179	2235.00	N_2O
48	238	2232.51	1178	2232.50	N_2O
49	241	2230.00	1177	2230.00	N_2O
50	247	2225.01	1175	2225.00	T
51	250	2222.52	1174	2222.50	T
52	253	2220.04	1173	2220.00	T, CO, N_2O
53	256	2217.56	1172	2217.50	CO, N_2O
54	259	2215.09	1171	2215.00	CO, N_2O
55	262	2212.63	1170	2212.50	CO, N_2O
56	265	2210.17	1169	2210.00	CO, N_2O
57	268	2207.71	1168	2207.50	T, CO, N_2O
58	271	2205.26	1167	2205.00	CO, N_2O
59	274	2202.82	1166	2202.50	T, CO, N_2O
60	277	2200.38	1165	2200.00	T, CO, N_2O
61	281	2197.13	1164	2197.50	CO, N_2O
62	284	2194.71	1163	2195.00	CO, N_2O
63	287	2192.29	1162	2192.50	CO
64	290	2189.87	1161	2190.00	CO, N_2O
65	293	2187.46	1160	2187.50	CO
66	296	2185.06	1159	2185.00	CO
67	299	2182.66	1158	2182.50	CO
68	302	2180.26	1157	2180.00	CO
69	305	2177.87	1156	2177.50	CO

Table 3 (*Continued*).

	CIRAS channel	CIRAS wavenumber	CrIS channel	CrIS wavenumber	Channel sensitivity
70	308	2175.49	1155	2175.00	CO
71	312	2172.32	1154	2172.50	CO
72	315	2169.95	1153	2170.00	CO
73	318	2167.58	1152	2167.50	CO
74	321	2165.22	1151	2165.00	CO
75	324	2162.86	1150	2162.50	CO
76	328	2159.73	1149	2160.00	CO
77	331	2157.38	1148	2157.50	CO
78	334	2155.04	1147	2155.00	CO
79	346	2145.74	6003	2145.50	H_2O
80	349	2143.42	5994	2143.25	H_2O
81	350	2142.65	5992	2142.75	H_2O
82	351	2141.88	5988	2141.75	H_2O
83	498	2034.45	5558	2034.25	H_2O
84	513	2024.09	5517	2024.00	H_2O
85	516	2022.03	5509	2022.00	H_2O
86	517	2021.34	5507	2021.50	H_2O
87	519	2019.97	5502	2020.25	H_2O
88	522	2017.92	5492	2017.75	H_2O
89	524	2016.56	5485	2016.00	H_2O
90	525	2015.88	5483	2015.50	H_2O
91	527	2014.51	5480	2014.75	H_2O
92	536	2008.41	5455	2008.50	H_2O
93	554	1996.30	5405	1996.00	H_2O
94	555	1995.63	5403	1995.50	H_2O
95	556	1994.97	5399	1994.50	H_2O
96	557	1994.30	5397	1994.00	H_2O
97	562	1990.97	5383	1990.50	H_2O
98	563	1990.31	5381	1990.00	H_2O
99	564	1989.64	5379	1989.50	H_2O
100	567	1987.65	5371	1987.50	H_2O
101	568	1986.99	5368	1986.75	H_2O

Acknowledgments

Grateful acknowledgment is made to the funding provided by the Disaster Relief Appropriations Act of 2013 (H.R. 152) and by the NOAA Quantitative Observing Systems Assessment Program (QOSAP), through the following NOAA grants: Cooperative Institute for Marine and Atmospheric Studies (CIMAS) Contributions to OAR Disaster Recovery Act Projects (NA14OAR4830103); Observing System Simulation Experiments (OSSEs) in support of Joint Center for Satellite Data Assimilation (JCSDA) contribution to NOAA's Data Gap Mitigation Strategy Assessment (NO14OAR4830157); Cooperative Institute for Meteorological Satellite Studies (CIMSS) Participation in NOAA Laboratory Activity for Observing System Simulation Experiments (NA14OAR4830094); and Establishment of a NOAA Laboratory Activity for Observing System Simulation Experiments (OSSEs) (NA14OAR4830105). This study was supported by NOAA grant NA14NES4320003 (Cooperative Institute for Climate and Satellites, CICS) at the University of Maryland/ESSIC.

References

1. C. Cardinali, "Forecast sensitivity to observation (FSO) as a diagnostic tool," Technical Memo 599, European Centre for Medium-Range Weather Forecasts (2009).
2. T. S. Pagano et al., "The CubeSat infrared atmospheric sounder (CIRAS), pathfinder for the earth observing nanosatellite-infrared (EON-IR)," in *30th Annual AIAA/USU SmallSat Conf.*, Logan, Utah (2016).
3. A. Poghosyan and A. Golkar, "CubeSat evolution: analyzing CubeSat capabilities for conducting science missions," *Prog. Aerosp. Sci.* **88**, 59–83 (2017).
4. E. Mabrouk, Ed., "What are SmallSats and CubeSats?, https://www.nasa.gov/content/what-are-smallsats-and-cubesats (7 August 2017).
5. J. M. English, A. C. Kren, and T. R. Peevey, "Improving winter storm forecasts with observing system simulation experiments (OSSEs). Part 2: evaluating a satellite gap with idealized and targeted dropsondes," *Earth Space Sci.* **5**(5), 176–196 (2018).
6. R. Gelaro et al., "Evaluation of the 7-km GEOS-5 nature run," Technical Report Series on Global Modeling and Data Assimilation 36, NASA Global Modeling and Assimilation Office, Greenbelt, Maryland (2014).
7. W. M. Putman et al., "A 7-km non-hydrostatic global mesoscale simulation for OSSEs with the Goddard Earth Observing System model (GEOS-5)," in *19th Conf. Integr. Observing and Assimilation Syst. Atmos., Oceans, and Land Surface (IOAS-AOLS)* (2015).
8. S.-A. Boukabara et al., "Community global observing system simulation experiment (OSSE) package (CGOP): description and usage," *J. Atmos. Oceanic Technol.* **33**(8), 1759–1777 (2016).
9. D. T. Kleist and I. Kayo, "An OSSE-based evaluation of hybrid variational-ensemble data assimilation for the NCEP GFS. Part II: 4DEnVar and hybrid variants," *Mon. Weather Rev.* **143**(2), 452–470 (2015).
10. S.-A. Boukabara et al., "Community global observing system simulation experiment (OSSE) package: CGOP. Part II: perfect observations simulation validation," *J. Atmos. Oceanic Technol.* **35**(1), 207–226 (2018).
11. S.-A. Boukabara et al., "Community global observing system simulation experiment (OSSE) package (CGOP): assessment and validation of the OSSE system using an OSSE/OSE intercomparison of summary assessment metrics," *J. Atmos. Oceanic Technol.* **35**(10), 2061–2078 (2018).
12. D. T. Kleist and K. Ide, "An OSSE-based evaluation of hybrid variational-ensemble data assimilation for the NCEP GFS. Part I: system description and 3D-hybrid results," *Mon. Weather Rev.* **143**(2), 433–451 (2015).
13. R. M. Errico et al., "Development and validation of observing-system simulation experiments at NASA's global modeling and assimilation office," *Q. J. R. Meteorolog. Soc.* **139**(674), 1162–1178 (2013).
14. N. C. Prive et al., "An observing system simulation experiment for the unmanned aircraft system data impact on tropical cyclone track forecasts," *Mon. Weather Rev.* **142**(11), 4357–4363 (2014).

15. L. P. Riishojgaard et al., "Observation system simulation experiments for a global wind observing sounder," *Geophys. Res. Lett.* **39**(17), L17805 (2012).
16. S.-A. Boukabara, K. Garrett, and V. K. Kumar, "Potential gaps in the satellite observing system coverage: assessment of impact on NOAA's numerical weather prediction overall skills," *Mon. Weather Rev.* **144**(7), 2547–2563 (2016).
17. T. S. Pagano et al., "Design and development of the CubeSat Infrared Atmospheric Sounder (CIRAS)," *Proc. SPIE* **10402**, 1040209 (2017).
18. Y. Chen, Y. Han, and F. Weng, "Comparison of two transmittance algorithms in the community radiative transfer model: application to AVHRR," *J. Geophys. Res.* **117**, D06206 (2012).
19. T. Zhu et al., "Synthetic radiance simulation and evaluation for a joint observing system simulation experiment," *J. Geophys. Res.* **117**, D23111 (2012).
20. X. Zhuge et al., "Dependence of simulation biases at AHI surface-sensitive channels on land surface emissivity over China," *J. Atmos. Oceanic Technol.* **35**(6), 1283–1298 (2018).
21. F. Rabier et al., "Channel selection methods for infrared atmospheric sounding interferometer radiances," *Q. J. R. Meteorol. Soc.* **128**, 1011–1027 (2002).
22. A. D. Collard, "Selection of IASI channels for use in numerical weather prediction," *Q. J. R. Meteorolog. Soc.* **133**(629), 1977–1991 (2007).
23. L. Ventress and A. Dudhia, "Improving the selection of IASI channels for use in numerical weather prediction," *Q. J. R. Meteorolog. Soc.* **140**(684), 2111–2118 (2014).
24. A. Gambacorta and C. D. Barnet, "Methodology and information content of the NOAA NESDIS operational channel selection for the cross-track infrared sounder (CrIS)," *IEEE Trans. Geosci. Remote Sens.* **51**(6), 3207–3216 (2013).
25. M. Matricardi, M. López-Puertas, and B. Funke, "Modeling of nonlocal thermodynamic equilibrium effects in the classical and principal component-based version of the RTTOV fast radiative transfer model," *J. Geophys. Res.* **123**(11), 5741–5761 (2018).

Yan Zhou is a postdoc at the Earth System Science Interdisciplinary Center, University of Maryland (UMD). She received her PhD degree in atmospheric science from the Department of Atmospheric and Oceanic Science, UMD. She is interested in data assimilation and numerical model prediction, validation, and bias estimation.

Biographies of the other authors are not available.